

Communication

# Molecularly Imprinted Polymer-Based Optical Sensor for Isopropanol Vapor

A. K. Pathak <sup>1</sup> , P. Limprapassorn <sup>2</sup>, N. Kongruttanachok <sup>3</sup> and C. Viphavakit <sup>1,\*</sup> 

<sup>1</sup> International School of Engineering (ISE), Intelligent Control Automation of Process Systems Research Unit, Chulalongkorn University, Bangkok 10330, Thailand

<sup>2</sup> Department of Laboratory Medicine, King Chulalongkorn Memorial Hospital, Thai Red Cross Society, Bangkok 10330, Thailand

<sup>3</sup> Department of Laboratory Medicine, Faculty of Medicine, Chulalongkorn University, Bangkok 10330, Thailand

\* Correspondence: charusluk.v@chula.ac.th

**Abstract:** Recent advances have allowed the monitoring of several volatile organic compounds (VOCs) in human exhaled breath, and many of them are being utilized as a biomarker to diagnose several diseases, including diabetes. Among several VOCs, isopropanol (IPA) has been reported as a common volatile compound in the exhaled breath of patients with type 1 and type 2 diabetes. In this article, an experimental approach is discussed to develop a highly selective and sensitive IPA vapor sensor system. The fabricated sensor is comprised of a small and portable glass slide coated with molecularly imprinted polymer containing specific binding sites compatible with IPA molecules. The developed sensor is based on the wavelength interrogation technique. The fabricated device is analyzed for the detection of IPA vapor with different concentrations varying from 50% to 100%. The sensor exhibits maximum sensitivities of 0.37, 0.30, and 0.62 nm/%IPA, respectively, for 30, 60, and 90 min, respectively, and an excellent sensitivity of 0.63 nm/%IPA for 120 min exposure along with good selectivity among a similar class of VOCs. The major features of the sensor i.e., small size, portability, cost-effectiveness, high sensitivity, and good selectivity, make it a potential candidate for diabetes monitoring. The promising results of the sensor illustrate its potential in diabetes monitoring applications.

**Keywords:** optical sensor; molecularly imprinted polymer; volatile organic compound; isopropanol; biomarker; diabetes



**Citation:** Pathak, A.K.; Limprapassorn, P.; Kongruttanachok, N.; Viphavakit, C. Molecularly Imprinted Polymer-Based Optical Sensor for Isopropanol Vapor. *J. Sens. Actuator Netw.* **2022**, *11*, 46. <https://doi.org/10.3390/jsan11030046>

Academic Editor: Marimuthu Palaniswami

Received: 8 July 2022

Accepted: 5 August 2022

Published: 9 August 2022

**Publisher's Note:** MDPI stays neutral with regard to jurisdictional claims in published maps and institutional affiliations.



**Copyright:** © 2022 by the authors. Licensee MDPI, Basel, Switzerland. This article is an open access article distributed under the terms and conditions of the Creative Commons Attribution (CC BY) license (<https://creativecommons.org/licenses/by/4.0/>).

## 1. Introduction

Investigations on volatile organic compound (VOC) vapors in exhaled breath have been evolving for several years with the utilization of various procedures and approaches. Breath analysis was introduced in ancient times when Hippocrates introduced the role of breath odor in identifying diseases and their stages, including uncontrolled diabetes, liver diseases, and kidney failure [1]. Afterward, in 1992, Michael reported the first literature work on breath tests in the field of medicine, which discussed the test's application in the diagnosis of various diseases. Later, in 2012, Minh et al. reported certain odors in human breath that are associated with specific diseases, e.g., the "fishy" smell is associated with renal failure [2]. In 1798, the "fruity" odor in exhaled breath was observed by John Gallo, which was later described as acetone in 1857 [3]. It was the first VOC biomarker used to predict the stages of diabetes. Thereafter, the monitoring and real-time analysis of VOC biomarkers from breath samples has been recognized as a new frontier for several diseases, including diabetes diagnostics and health inspections.

The exhaled breath of patients with type-1 and type-2 diabetes contains several other VOCs besides acetone, such as ethanol, isopropanol (IPA), and methanol [4]. However, acetone has already been well explored for its presence in other diseases, such as lung

cancer [5], cystic fibrosis [6], and asthma [7], which may lead to misdiagnosis. Hence, several researchers have focused on other VOC biomarkers to accurately identify diabetes, e.g., IPA [8–10]. The concentrations of exhaled IPA in a diabetic group (mean 85.44 ppbv) were observed to be significantly higher as compared to the healthy groups (mean 17.99 ppbv,  $p < 0.001$ ) [9].

The most conventional techniques for VOC monitoring include gas chromatography mass spectrometry (GCMS) [11]. Although these approaches allow a high precision and resolution for VOC detection, they are expensive and large in size. Moreover, a skilled technician is required to operate the machine, which can limit their onsite use and real-time monitoring. In addition, GCMS requires sample preparation, which can be time consuming. To overcome these limitations, several researchers have explored the role of conducting polymers, such as polydimethylsiloxane [12–14], polyaniline [15], and molecularly imprinted polymer (MIP) [16], in gas sensing. Conducting polymers and their derivatives have been used as the active sensing layer for gases since the 1980s [17,18]. Such polymers possess several interesting features for gas sensing, including their fast response time due to the swelling and shrinkage phenomenon [19]. They can achieve high sensitivity and selectivity at room temperature (25 °C) [20–26]. Among several polymers, a recent study reported MIP as a highly selective and sensitive material for VOC detection [16].

Molecular imprinting is a technique that is widely used for the synthesis of polymer matrices with modified binding sites for the detection of a specific target, known as a template molecule [27]. The procedure is performed by polymerizing a mixture of the target template (atoms, ions, ionic assembly, molecule, or macromolecular) with a particular monomer and cross-linking agent. Later, the target template is washed out from the polymerized medium using a removal reagent. The process leaves nanocavities with an identical shape and size as the target template in the polymer, which act as the recognition site for the same target molecule. The exact shape and size of cavities make the recognition of identical template molecules highly selective. This technique is very promising in the development of vapor sensor systems with high selectivity and good sensitivity [28,29].

The present study proposes a VOC vapor sensor system utilizing MIP as the selective and sensitive material. A very compact size of the glass slide was used as a sensing platform for the deposition of MIP. The sensing configuration was based on the wavelength interrogation technique, and the analyses were performed over IPA concentrations varying from 20% to 100%. Furthermore, the exposure time was varied to optimize the time to achieve the highest sensitivity. The sensing performance was characterized in terms of sensitivity, selectivity, and repeatability. To the best of our knowledge, this proposed sensor is the first of its kind developed for IPA vapor detection that can be implemented for diabetes monitoring applications.

## 2. Materials and Methods

### 2.1. Materials

Ethylene glycol dimethacrylate (EGDMA), 2,2'-azobis-isobutyronitrile (AIBN), and 3-(trimethoxysilyl) propyl methacrylate (3TMPMA) were obtained from Sigma Aldrich, Bangkok Thailand. Meanwhile, hydrochloric acid (HCl), sodium hydroxide (NaOH), and toluene (C<sub>7</sub>H<sub>8</sub>) were obtained from Merck, Bangkok, Thailand. Methacrylic acid (MAA) and IPA (C<sub>3</sub>H<sub>8</sub>O) were obtained from TCI and QReC, respectively. All chemicals were of analytical grade and used without further purifications.

### 2.2. Synthesis of IPA–MIP

The MIP for IPA monitoring IPA–MIP was prepared using a classical non-covalent approach. Here, IPA was used as the target template. MAA, EGDMA, and AIBN were used as the monomer, crosslinker, and initiator, respectively [30]. The pre-polymeric solution for IPA–MIP was obtained by mixing IPA templates (21 µL), MAA (45 µL), EGDMA (188 µL), and AIBN (20 µL) in a small vessel. The amount of crosslinker content plays a very important role in polymerization: more than 60% content yields a hard and cracked surface,

and less than 60% results in a non-smooth and semi-liquid surface. Thereafter, the mixture was uniformly dispersed via sonication and de-aerated with nitrogen for 5 min to obtain a homogenous and transparent solution. The synthesis step of the IPA–MIP solution is shown in Figure 1. Solutions for the nonimprinted polymer solutions for the nonimprinted polymer (NIP) were synthesized similarly in the absence of an IPA template molecule.

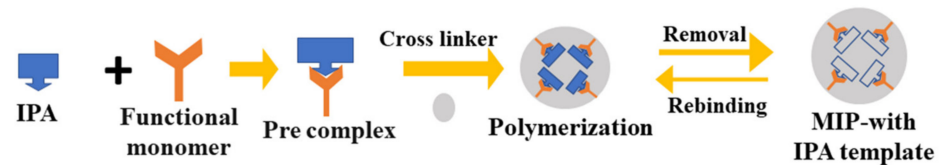


**Figure 1.** Schematic diagram of the synthesis procedure.

### 2.3. Sensor Fabrication

Sensor fabrication requires pre-surface functionalization on the substrate surface. To prepare the glass substrate for the IPA–MIP deposition, a glass slide of size  $1 \times 0.3$  cm was cleaned by immersing it in 0.1% HCl for 30 min and then in NaOH and for 1 h [31]. After cleaning, the glass slide was washed with DI water and dried under nitrogen. Prior to the deposition of IPA–MIP, the vinylization of the glass surface is needed to introduce a vinyl group to improve the adhesion of IPA–MIP on the substrate. The vinylization step was performed by immersing the glass slide into 10% of 3TMPMA in toluene for 1 h [32]. After functionalization, the glass slide was placed in an oven at 70 °C for 2 h. The glass slide was then coated with the IPA–MIP solution through the drop-casting technique [33]. A small drop of IPA–MIP was placed on the glass slide to cover the whole surface and subsequently polymerized under UV irradiation with  $\lambda = 365$  nm. After the polymerization, the glass slide was left for 24 h at room temperature. Then, the IPA template was extracted by sonicating the sample in ethanol for 1 min [30]. This template removal step allows binding sites to successfully entrap IPA molecules. To prepare for characterization, the sensor was left for 48 h at room temperature to ensure the complete evaporation of the washing solvent from the surface and avoid the possible mixing of two VOCs. The fabrication procedure of the sensor coated with polymerized IPA–MIP is shown in Figure 2.

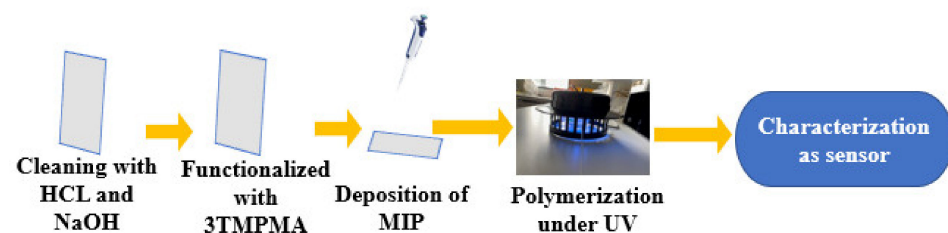


**Figure 2.** Schematic of sensor fabrication including surface functionalization and polymerization.

## 3. Experimental

A schematic diagram of the experimental setup used to monitor the sensing response of the sensor is shown in Figure 3a. The sensing performance of sensor was analyzed using UV-Vis spectrophotometer (LAMBDA 850+) containing a 50-watt halogen lamp operates in the wavelength range varying from 100 to 900 nm with wavelength accuracy of  $\pm 0.080$  nm and a resolution of 0.05 nm. The experimental setup consists of a UV-Vis spectrophotometer (with source and detector inbuilt) and quartz cuvette. To monitor the sensing response, the sensor was attached to the inner wall of the cuvette filled with various IPA concentrations. Thereafter, the whole assembly was sealed with paraffin tape for the maximum interaction of IPA vapor with the IPA–MIP and placed in a UV-Vis spectrophotometer to measure the sensing response. When the light was launched from the source, it propagated to the detector through an IPA–MIP-coated sensing configuration. The entrapment of IPA molecules in the IPA–MIP film caused the changes in the refractive index and other optical

properties of the IPA–MIP, i.e., light absorption and transmission spectrum, which can be recorded by the detector. The sensor is based on the wavelength interrogation technique; hence, the shift in transmitted spectra is presented in this paper. The actual setup for the characterization is shown in Figure 3b. It includes the actual assembly of the cuvette and sensor and actual size of the fabricated sensor. The red arrow in Figure 3b shows the direction of the light propagation from the source to the detector. For the characterization, the cuvette was filled with 300  $\mu\text{L}$  of the measurand. All the analyses were performed at room temperature. The dissolution of IPA in the cuvette obeys Henry's gas law, which defines the solubility of IPA in water according to the partial pressure of gaseous IPA [34]. The Henry's law constant is a temperature and pressure dependent parameter [35]. In our case, we consider room temperature (25  $^{\circ}\text{C}$ ) throughout the investigations.

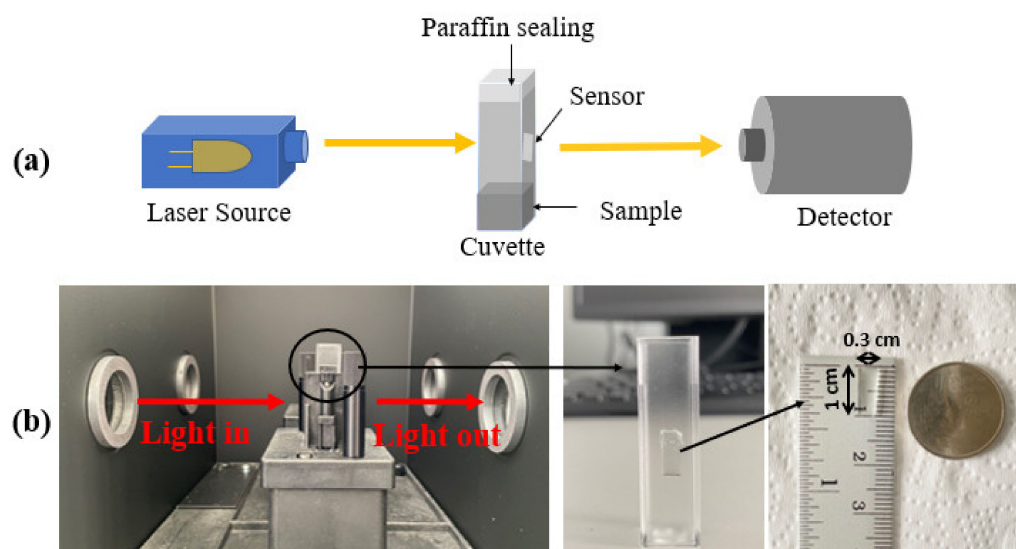


**Figure 3.** (a) Schematic diagram of the measurement used to analyze the sensing response of the sensor; (b) image of the actual setup and sensor size.

## 4. Material Characterization

### 4.1. FTIR Analysis

Material characterizations of the fabricated sensor are required to validate the polymerization and surface morphology. Fourier-transform infrared spectroscopy (FTIR) is a useful analytical tool to identify polymerization, which is important for determining storage, exhibition, loan, and treatment conditions [36]. Figure 4 illustrates the comparative FTIR spectrum for the monomer (MAA), NIP, and IPA–MIP. The peak at  $2963\text{ cm}^{-1}$  corresponded to the C–H stretching vibration in MAA. The next peak at  $1689\text{ cm}^{-1}$  was assigned to the C=O group, and the peaks at  $1631$ ,  $1375$ , and  $1200\text{ cm}^{-1}$ , were assigned to the C=C, O–H, and C–O groups for MAA, respectively.

The spectra of the NIP and IPA–MIP remained for several groups, such as the C–H group, located at peaks  $2958$ ,  $2957$ , and  $2957\text{ cm}^{-1}$ . Meanwhile, C=O was assigned at peak  $1716\text{ cm}^{-1}$  for NIP, and C–O was assigned at peak  $1143\text{ cm}^{-1}$ , which illustrate the existence of an EGDMA cross-linker. The O–H bending vibration at  $1375\text{ cm}^{-1}$  confirmed the presence of carboxylic acid groups in NIP and IPA–MIP. The NIP and IPA–MIP were successfully polymerized, which is confirmed by the reduced intensity of C=C at peak  $1631\text{ cm}^{-1}$ . The disappearance of this peak ( $1631\text{ cm}^{-1}$ ) strongly indicates the polymerization between the cross-linkers and monomers [37]. The polymerization process is marked with the lower transmittance intensity of C=C stretching ( $1635\text{ cm}^{-1}$ ) and double-bond C=O bending ( $553\text{ cm}^{-1}$ ) in the NIP and IPA–MIP compared to the intensity of the double-bond in the MAA monomer.

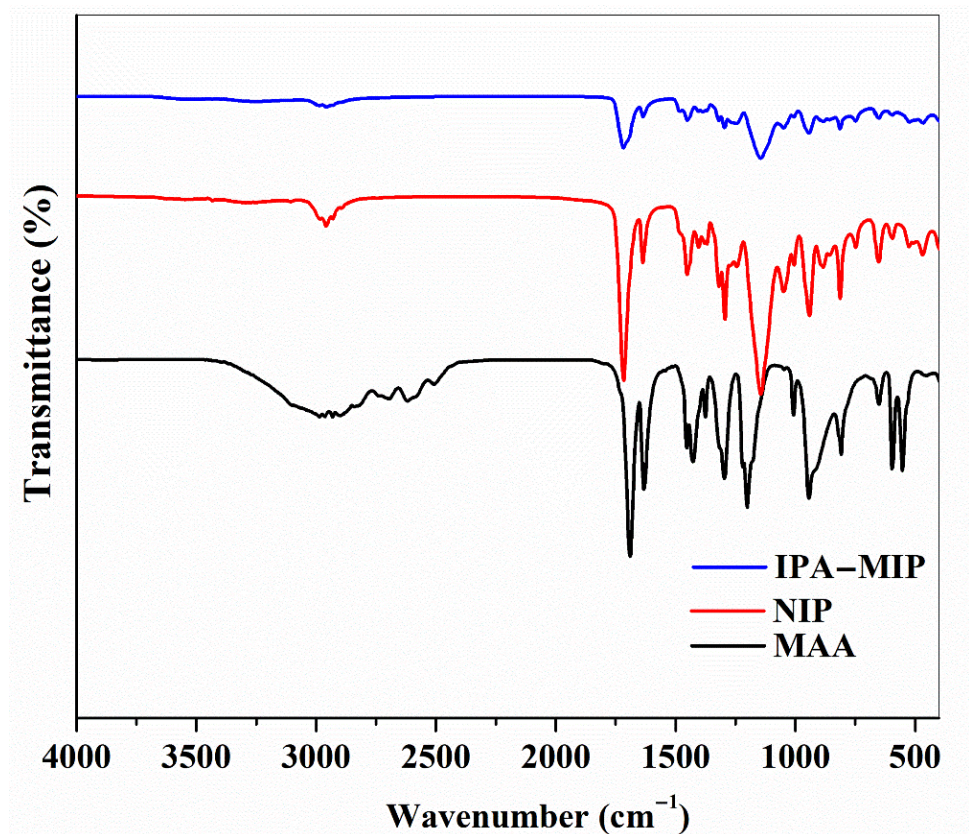


**Figure 4.** FTIR analysis for the IPA-MIP, NIP, and MAA.

#### 4.2. Morphological Study of the IPA-MIP and NIP

Field emission scanning electron microscopy (FESEM) and atomic force microscopy (AFM) are crucial and valuable analysis approaches for a clear understanding of the surface morphology and roughness of polymers. The morphology of the representative NIP and IPA-MIP on the glass slides was examined via FESEM ((JSM-7610F) JEOL) at 100,000 times magnifications over a bar scale of 100 nm. Figure 5 shows a clear image of surface morphology of the polymer. In Figure 5a, the NIP surface is relatively smoother and less porous as compared to that of the IPA-MIP shown in Figure 5b. The regular texture for NIP was obtained because there is no template in the synthesis leading to no specific binding sites for IPA. Meanwhile, the crack and porosity on the IPA-MIP surface occurred due to the successful removal of the IPA templates. The increase in the wrinkled structure and surface roughness in IPA-MIP images can be attributed to the increase in the surface area due to the accommodation of the IPA template [38]. The uniform layer of the IPA-MIP is the main reason allowing effective template extraction and quick binding kinetics because specific binding sites are exposed to the surface [39], resulting in the good performance of IPA-MIP particles.

An AFM analysis was performed for the same samples to obtain an intuitive view of the surface roughness. Figure 6a,b illustrate the 3D image of the analyzed surface area of  $10 \times 10 \mu\text{m}^2$  for the NIP and IPA-MIP, respectively. The 3D image clearly shows a remarkable difference in the surface roughness of the NIP and IPA-MIP, which can be defined in terms of the root-mean-square (RMS) value. An RMS roughness of 1.29 nm obtained for the NIP, which was later increased to 1.76 nm following the formation of the binding sites of IPA-MIP.

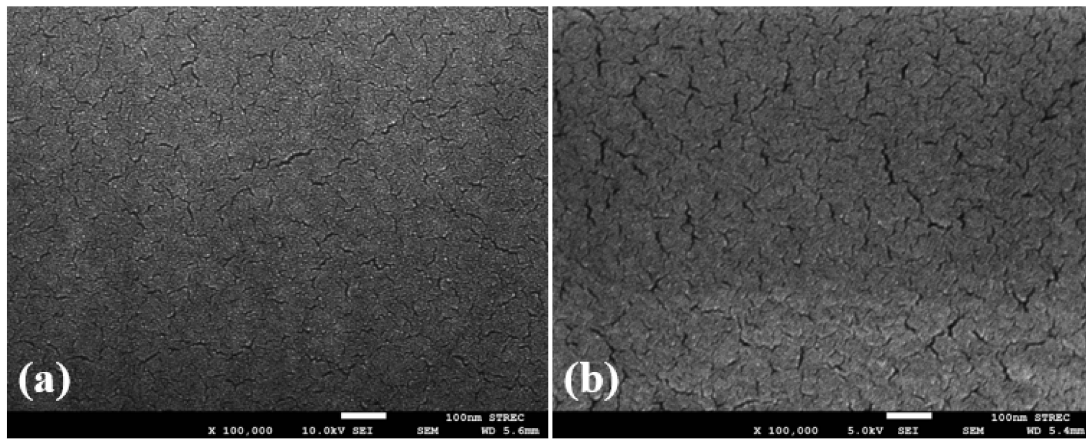


**Figure 5.** FESEM images of (a) NIP and (b) IPA-MIP.

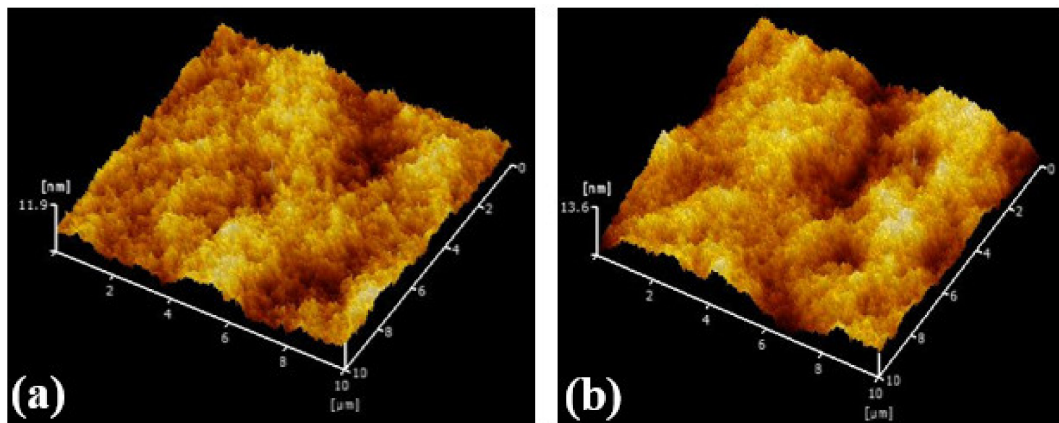


**Figure 6.** AFM image analysis for (a) the NIP and (b) IPA-MIP.

## 5. Results and Discussion

### 5.1. Saturation Time

Here, concentrations 50%, 80%, and 100% mean that the measurand contains 50%, 80%, and 100% of IPA in 50%, 20%, and 0% of deionized (DI) water in a 300  $\mu$ L solution, respectively. To prepare these concentrations, an appropriate amount of IPA was mixed with DI water and stirred well to obtain a homogenous solution before the analysis. During the characterization, the fabricated sensor was initially investigated for its saturation time with 100% and 50% IPA concentrations. To monitor the saturation time, the sensor was placed inside the cuvette, and the absorption spectra were recorded for 120 min, as shown in Figure 7. As shown in the figure, a sharp increase in the absorbance appeared up to 60 min for both concentrations due to the accommodation of the IPA molecule on the top layer of the MIP. After 60 min, a slow increment occurred due to the diffusion of IPA vapor into the porous IPA-MIP, allowing IPA to be accommodated in the inner cavities. The absorbance kept slightly increasing with time up to 120 min before the condensation of IPA vapor occurs due to the heat from the source. This result might be possible due to the greater number of nanocavities available compared to the IPA molecules in vapor. Therefore, accommodating all IPA molecules in each of their cavities may take a long time. Hence, this fabricated sensor has a potential for a long continuous monitoring time.

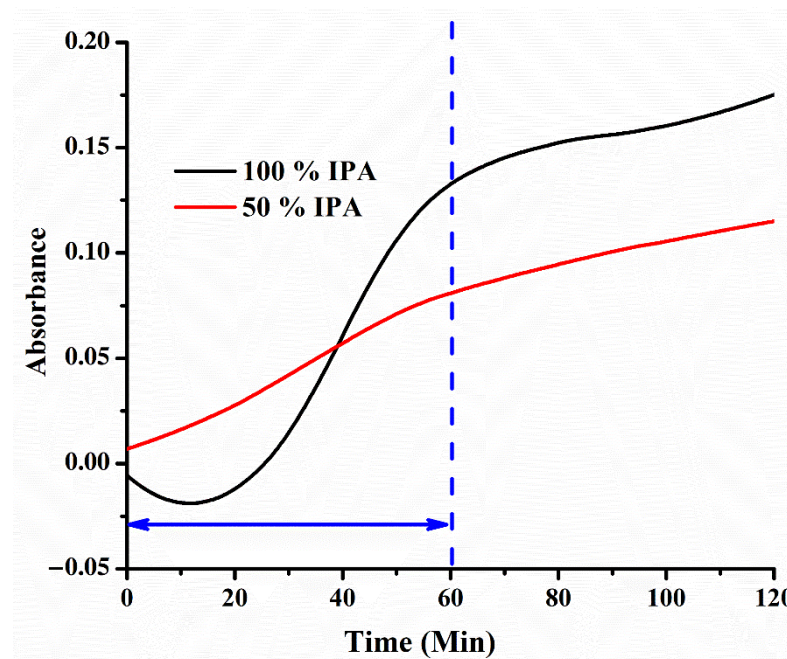


**Figure 7.** Saturation response of the sensor corresponding to 50% and 100% IPA concentrations.

### 5.2. Sensitivity

The transmittance spectra of the IPA–MIP sensing configuration were recorded when the sensor was exposed to 50%, 80%, and 100% IPA concentrations at various exposure times varying from 30 min to 120 min at an interval of 30 min. The experiment was designed to optimize the exposure time required for the sensor to selectively entrap IPA molecules in most of the available nanocavities. At exposure times of 30, 60, 90, and 150 min, the transmittance spectra exhibited a small shift in the wavelength dip with increasing IPA concentrations. However, each exposure time exhibited a good redshift in the dip wavelengths due to the availability of specific binding sites in IPA–MIP. However, exposure time of 120 min led to a larger shift in the dip wavelength as compared to other exposure times. It might be possible that exposure time of 120 min is enough for the maximum entrapment of IPA molecules in available cavities throughout the MIP layer. Figure 8 illustrates the shift in transmittance spectra for 120 min exposure time at various IPA concentrations. Figure 8 shows that varying the IPA concentration exhibits a good redshift. For a concentration lower than 50%, there is no significant variation to any exposure time. This is due to the less IPA concentration, which may require a large vaporization time (i.e., <150 min).

Figure 9 illustrates a linear relation between the IPA concentration and dip wavelength. The calibration plot shown in Figure 9 illustrates a good linear relationship ( $r^2 = 0.95$ ) between the IPA concentration and corresponding wavelength dip. The sensitivity ( $S$ ) of the sensor is defined as the variation in dip wavelength per unit change in the IPA concentration in DI water, which can be explained by the following relation [40–42]:

$$S = \Delta\lambda_{dip} / \Delta concentration_{IPA} \text{ (nm/\%IPA)} \tag{1}$$

where  $\Delta\lambda_{dip}$  shows the shift in wavelength and  $\Delta concentration_{IPA}$  shows the variation in the IPA concentration in DI water. The sensitivity of the sensor was calculated via linear fitting, as shown in Figure 9. Exposure time of 120 min achieved the highest sensitivity of 0.63 nm/%IPA at room temperature. Meanwhile, other exposure times, such as 30, 60, and 90 min, attained the maximum sensitivity of 0.37 nm/%IPA, 0.30 nm/%IPA, and 0.62 nm/%IPA, respectively. Hence, the investigation confirms that it takes 120 min for

IPA molecules to selectively attach with their size specific cavities and hence give a high sensitivity to devices.

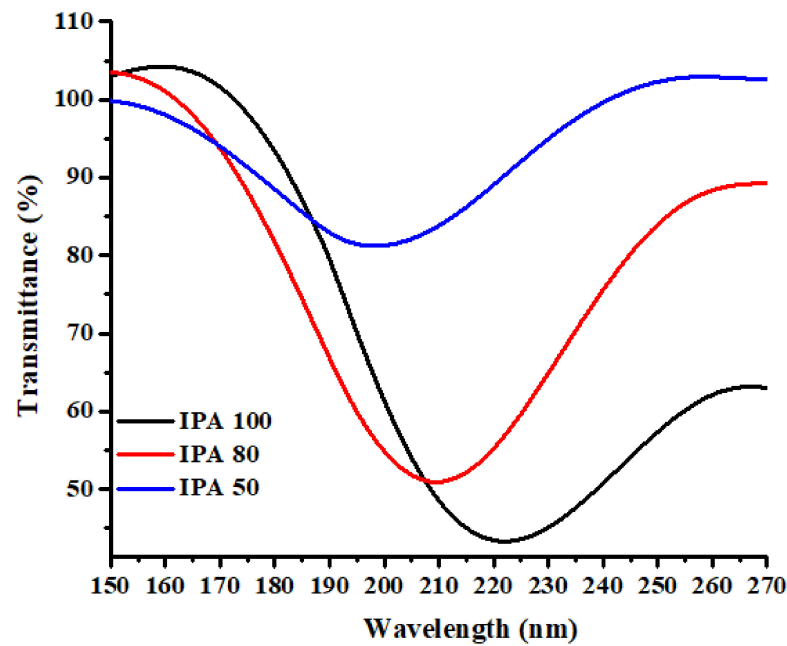


Figure 8. Transmittance spectra at various concentrations.

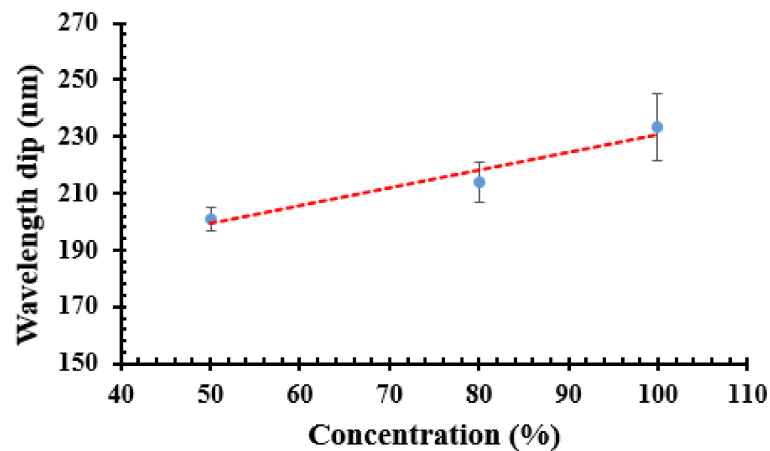


Figure 9. Sensitivities of the fabricated device.

At 50% IPA concentration, an error bar of  $\pm 1.0\%$  was calculated from the standard deviation between the measurements. A smaller variation at the lower concentration of IPA solution can be due to a larger ratio between nanocavities and IPA molecules. Therefore, a constant dynamic change of the peak wavelength can be achieved, leading to a smaller variation. At the higher concentration, the ratio between nanocavities and IPA molecules is smaller as the number of IPA molecules is increased, but the number of nanocavities remains the same. However, a maximum error bar of  $\pm 2.5\%$  at 100% IPA concentration was obtained for this sensor, which is considered to be a good repeatability and consistency system.

To confirm the response of the IPA-MIP, a similar experiment was also performed over an NIP-coated sensing configuration. The wavelength shift for NIP is very small, i.e., 1.1 nm. Therefore, the sensitivity of the IPA-MIP sensor is significantly higher than that of the NIP sensor. The result suggests that the recognition capability in MIP is more effective for IPA sensing than the NIP.

### 5.3. Selectivity

After analyzing the sensing response of the sensor, the same sensor was examined to study its selectivity response. The adsorption properties of the IPA–MIP sensor with other VOC biomarkers of diabetes were studied. The nano cavities in the polymer have excellent matching with the IPA template in terms of size and shape, allowing the polymer to selectively adsorb IPA vapor. To investigate the selectivity of the IPA–MIP-coated sensor, the adsorption experiment was performed using 300  $\mu\text{L}$  of pure ethanol, methanol, and IPA. The choices of VOCs were based on their similar class of alcohols available in the exhaled breath of patients with diabetes. To monitor the selectivity of the sensor, 300  $\mu\text{L}$  of pure VOC solutions were placed in the sealed cuvette, as discussed in Section 3. Figure 10 illustrates the absorption property of the sensor for pure IPA, methanol, and ethanol. The presence of IPA apparently produces a stronger absorption intensity of 0.54% as shown by the black line, compared to methanol (0.48%) and ethanol (0.43%) shown by the red and blue lines, respectively. The stronger intensity for IPA occurs due to the selective absorption of IPA in IPA–MIP nanocavities which confirm good selectivity feature of the IPA–MIP [43]. The interaction of methanol and ethanol also leads to the absorbance spectra due to the swelling shrinkage phenomenon of polymer, leading to the change in its refractive index.

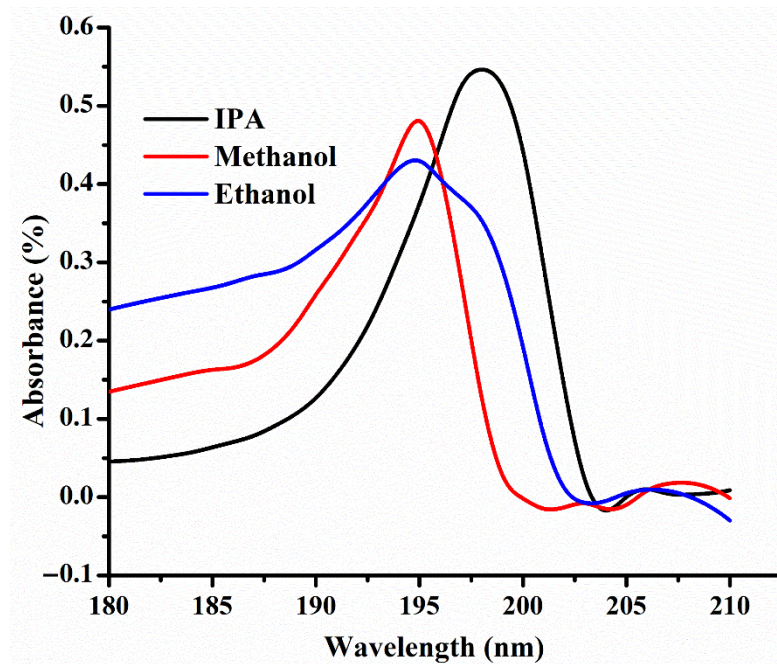


Figure 10. Sensing response of the sensor in the presence of various VOCs.

## 6. Conclusions

In the present study, a cost-effective optical vapor sensor system on a glass slide coated with IPA–MIP was fabricated and experimentally validated for the selective detection of IPA vapor. An IPA–MIP film on the glass substrate was deposited as an adsorbent for IPA vapor. The sensing configuration was optimized in terms of synthesis, polymerization, and exposure time. The sensor comprises of an IPA–MIP layer deposited over a small glass slide ( $1 \times 0.3$  cm) via a drop-casting method to attain the film uniformity. The sensor is based on the wavelength interrogation technique. The obtained results exhibit that the fabricated sensor has a good wavelength shift for a high IPA concentration and achieve a maximum sensitivity of 0.63 nm/%IPA with a good linear response of 0.95 for 120 min of IPA exposure. The fabricated device was also tested in the presence of other VOCs, resulting in the highest adsorption for IPA compared to other VOCs. Hence, the promising selectivity and sensitivity illustrate that the fabricated sensor could be helpful for the future

development of gas sensors for IPA vapor biomarker detection and breath monitoring of individuals suffering from diabetes.

**Author Contributions:** Conceptualization, C.V.; methodology, A.K.P. and C.V.; validation, A.K.P. and P.L.; formal analysis, A.K.P.; investigation, A.K.P.; resources, N.K. and C.V.; writing—original draft preparation, A.K.P.; writing—review and editing, C.V.; supervision, C.V.; project administration, N.K. and C.V.; funding acquisition, C.V. All authors have read and agreed to the published version of the manuscript.

**Funding:** This work is supported by the Second Century Fund (C2F), Chulalongkorn University, and Rachadapisek Sompote Fund for Intelligent Control Automation of Process Systems Research Unit, Chulalongkorn University.

**Informed Consent Statement:** Not applicable.

**Data Availability Statement:** Not applicable.

**Acknowledgments:** The authors are also thankful to Roli Verma, University of Lucknow, India, and Nunzio Cennamo, University of Campania, Italy, for the fruitful discussion over the synthesis part.

**Conflicts of Interest:** The authors declare no conflict of interest.

## References

1. Phillips, M. Breath Tests in Medicine. *Sci. Am.* **1992**, *267*, 74–79. [[CrossRef](#)] [[PubMed](#)]
2. Minh, T.D.C.; Blake, D.R.; Galassetti, P.R. The clinical potential of exhaled breath analysis for diabetes mellitus. *Diabetes Res. Clin. Pract.* **2012**, *97*, 195–205. [[CrossRef](#)] [[PubMed](#)]
3. Crofford, O.B.; Mallard, R.E.; Winton, R.E.; Rogers, N.L.; Jackson, J.C. Acetone in breath and blood. *Trans. Am. Clin. Climatol. Assoc.* **1977**, *88*, 128–139. [[PubMed](#)]
4. Leopold, J.H.; van Hooijdonk, R.T.; Sterk, P.J.; Abu-Hanna, A.; Schultz, M.J.; Bos, L.D. Glucose prediction by analysis of exhaled metabolites—A systematic review. *BMC Anesthesiol.* **2014**, *14*, 46. [[CrossRef](#)]
5. Machado, R.F.; Laskowski, D.; Deffenderfer, O.; Burch, T.; Zheng, S.; Mazzone, P.J.; Mekhail, T.; Jennings, C.; Stoller, J.K.; Pyle, J.; et al. Detection of Lung Cancer by Sensor Array Analyses of Exhaled Breath. *Am. J. Respir. Crit. Care Med.* **2005**, *171*, 1286–1291. [[CrossRef](#)]
6. Barker, M.; Hengst, M.; Schmid, J.; Buers, H.-J.; Mittermaier, B.; Klemp, D.; Koppmann, R. Volatile organic compounds in the exhaled breath of young patients with cystic fibrosis. *Eur. Respir. J.* **2006**, *27*, 929–936. [[CrossRef](#)]
7. Dragonieri, S.; Schot, R.; Mertens, B.J.A.; le Cessie, S.; Gauw, S.A.; Spanevello, A.; Resta, O.; Willard, N.P.; Vink, T.J.; Rabe, K.F.; et al. An electronic nose in the discrimination of patients with asthma and controls. *J. Allergy Clin. Immunol.* **2007**, *120*, 856–862. [[CrossRef](#)]
8. Molina, D.K. A Characterization of Sources of Isopropanol Detected on Postmortem Toxicologic Analysis. *J. Forensic Sci.* **2010**, *55*, 998–1002. [[CrossRef](#)]
9. Li, W.; Liu, Y.; Liu, Y.; Cheng, S.; Duan, Y. Exhaled isopropanol: New potential biomarker in diabetic breathomics and its metabolic correlations with acetone. *RSC Adv.* **2017**, *7*, 17480–17488. [[CrossRef](#)]
10. Pathak, A.K.; Viphavakit, C. VOC biomarker monitoring for diabetes through exhaled breath using Ag/P-TiO<sub>2</sub> composite plasmonic sensor. *IEEE Sens. J.* **2021**, *21*, 22631–22637. [[CrossRef](#)]
11. Lerner, B.M.; Gilman, J.B.; Aikin, K.C.; Atlas, E.L.; Goldan, P.D.; Graus, M.; Hendershot, R.; Isaacman-VanWertz, G.A.; Koss, A.; Kuster, W.C.; et al. An improved, automated whole air sampler and gas chromatography mass spectrometry analysis system for volatile organic compounds in the atmosphere. *Atmos. Meas. Tech.* **2017**, *10*, 291–313. [[CrossRef](#)]
12. Endo, T.; Yanagida, Y.; Hatsuzawa, T. Colorimetric detection of volatile organic compounds using a colloidal crystal-based chemical sensor for environmental application. *Sens. Actuators B Chem.* **2007**, *125*, 589–595. [[CrossRef](#)]
13. Viphavakit, C.; Patchoo, W.; Boonruang, S.; Themistos, C.; Komodromos, M.; Mohammed, W.S.; Rahman, B.M.A. Demonstration of Polarization-Independent Surface Plasmon Resonance Polymer Waveguide for Refractive Index Sensing. *J. Light. Technol.* **2017**, *35*, 3012–3019. [[CrossRef](#)]
14. Viphavakit, C.; Atthi, N.; Boonruang, S.; Themistos, C.; Komodromos, M.; Mohammed, W.S.; Rahman, B.M.A. Realization of a polymer nanowire optical transducer by using the nanoimprint technique. *Appl. Opt.* **2014**, *53*, 7487. [[CrossRef](#)]
15. Vu, D.L.; Lin, T.-F.; Lin, T.-H.; Wu, M.-C. Highly-Sensitive Detection of Volatile Organic Compound Vapors by Electrospun PANI/P3TI/PMMA Fibers. *Polymers* **2020**, *12*, 455. [[CrossRef](#)]
16. Herdes, C.; Sarkisov, L. Computer Simulation of Volatile Organic Compound Adsorption in Atomistic Models of Molecularly Imprinted Polymers. *Langmuir* **2009**, *25*, 5352–5359. [[CrossRef](#)]
17. Bai, H.; Shi, G. Gas Sensors Based on Conducting Polymers. *Sensors* **2007**, *7*, 267–307. [[CrossRef](#)]
18. Pathak, A.K.; Viphavakit, C. A Review on All-optical Fiber-based VOC sensors: Heading Towards the Development of Promising Technology. *Sens. Actuators A Phys.* **2022**, *338*, 113455. [[CrossRef](#)]

19. Swargiary, K.; Jolivot, R.; Mohammed, W.S. Demonstration of a Polymer-Based Single Step Waveguide by 3D Printing Digital Light Processing Technology for Isopropanol Alcohol-Concentration Sensor. *Photonic Sens.* **2022**, *12*, 10–12. [[CrossRef](#)]
20. Wang, Y.; Huang, Y.; Bai, H.; Wang, G.; Hu, X.; Kumar, S.; Min, R. Biocompatible and Biodegradable Polymer Optical Fiber for Biomedical Application: A Review. *Biosensors* **2021**, *11*, 472. [[CrossRef](#)]
21. Leal-Junior, A.; Frizzera, A.; Marques, C. A fiber Bragg gratings pair embedded in a polyurethane diaphragm: Towards a temperature-insensitive pressure sensor. *Opt. Laser Technol.* **2020**, *131*, 106440. [[CrossRef](#)]
22. Leal-Junior, A.G.; Frizzera, A.; Marques, C. Thermal and Mechanical Analyses of Fiber Bragg Gratings-Embedded Polymer Diaphragms. *IEEE Photonics Technol. Lett.* **2020**, *32*, 623–626. [[CrossRef](#)]
23. Pandey, P.S.; Raghuwanshi, S.K.; Kumar, S. Recent Advances in Two-Dimensional Materials-Based Kretschmann Configuration for SPR Sensors: A Review. *IEEE Sens. J.* **2022**, *22*, 1069–1080. [[CrossRef](#)]
24. Nadeem, M.D.; Raghuwanshi, S.K.; Kumar, S. Recent Advancement of Phase Shifted Fiber Bragg Grating Sensor for Ultrasonic Wave Application: A Review. *IEEE Sens. J.* **2022**, *22*, 7463–7474. [[CrossRef](#)]
25. Pathak, A.K.; Singh, V.K. A wide range and highly sensitive optical fiber pH sensor using polyacrylamide hydrogel. *Opt. Fiber Technol.* **2017**, *39*, 43–48. [[CrossRef](#)]
26. Gangwar, R.K.; Bhardwaj, V.; Singh, V.K. Magnetic field sensor based on selectively magnetic fluid infiltrated dual-core photonic crystal fiber. *Opt. Eng.* **2016**, *55*, 026111. [[CrossRef](#)]
27. Pesavento, M.; Zeni, L.; de Maria, L.; Alberti, G.; Cennamo, N. SPR-Optical Fiber-Molecularly Imprinted Polymer Sensor for the Detection of Furfural in Wine. *Biosensors* **2021**, *11*, 72. [[CrossRef](#)]
28. Verma, R.; Gupta, B.D. Fiber optic SPR sensor for the detection of 3-pyridinecarboxamide (vitamin B3) using molecularly imprinted hydrogel. *Sens. Actuators B Chem.* **2013**, *177*, 279–285. [[CrossRef](#)]
29. Verma, R.; Gupta, B.D. Optical fiber sensor for the detection of tetracycline using surface plasmon resonance and molecular imprinting. *Analyst* **2013**, *138*, 7254. [[CrossRef](#)]
30. Cennamo, N.; D'Agostino, G.; Pesavento, M.; Zeni, L. High selectivity and sensitivity sensor based on MIP and SPR in tapered plastic optical fibers for the detection of l-nicotine. *Sens. Actuators B Chem.* **2014**, *191*, 529–536. [[CrossRef](#)]
31. Koster, E.H.M.; Crescenzi, C.; den Hoedt, W.; Ensing, K.; de Jong, G.J. Fibers Coated with Molecularly Imprinted Polymers for Solid-Phase Microextraction. *Anal. Chem.* **2001**, *73*, 3140–3145. [[CrossRef](#)]
32. Lépinay, S.; Ianoul, A.; Albert, J. Molecular imprinted polymer-coated optical fiber sensor for the identification of low molecular weight molecules. *Talanta* **2014**, *128*, 401–407. [[CrossRef](#)] [[PubMed](#)]
33. Hijazi, H.Y.; Bottaro, C.S. Analysis of thiophenes in seawater: Molecularly imprinted polymer thin-film extraction with desorption electrospray ionization mass spectrometry. *Int. J. Mass Spectrom.* **2019**, *443*, 9–15. [[CrossRef](#)]
34. Liu, L.; Hao, F.; Morgan, S.P.; Correia, R.; Norris, A.; Korposh, S. A reflection-mode fibre-optic sensor for breath carbon dioxide measurement in healthcare. *Sens. Bio-Sens. Res.* **2019**, *22*, 100254. [[CrossRef](#)]
35. Wiebe, R.; Gaddy, V.L. The Solubility of Carbon Dioxide in Water at Various Temperatures from 12 to 40° and at Pressures to 500 Atmospheres. *Critical Phenomena. J. Am. Chem. Soc.* **1940**, *62*, 815–817. [[CrossRef](#)]
36. Bell, J.; Nel, P.; Stuart, B. Non-invasive identification of polymers in cultural heritage collections: Evaluation, optimisation and application of portable FTIR (ATR and external reflectance) spectroscopy to three-dimensional polymer-based objects. *Herit. Sci.* **2019**, *7*, 95. [[CrossRef](#)]
37. Asman, S.; Mohamad, S.; Sarih, N. Exploiting  $\beta$ -Cyclodextrin in Molecular Imprinting for Achieving Recognition of Benzylparaben in Aqueous Media. *Int. J. Mol. Sci.* **2015**, *16*, 3656. [[CrossRef](#)]
38. Chatterjee, T.N.; Roy, R.B.; Tudu, B.; Pramanik, P.; Deka, H.; Tamuly, P.; Bandyopadhyay, R. Detection of theaflavins in black tea using a molecular imprinted polyacrylamide-graphite nanocomposite electrode. *Sens. Actuators B Chem.* **2017**, *246*, 840–847. [[CrossRef](#)]
39. Mane, S.; Ponrathnam, S.; Chavan, N. Design and synthesis of cauliflower-shaped hydroxyl functionalized core-shell polymer. *Des. Monomers Polym.* **2015**, *18*, 723–733. [[CrossRef](#)]
40. Pathak, A.K.; Singh, V.K. Theoretical assessment of D-shaped optical fiber chemical sensor associated with nanoscale silver strip operating in near-infrared region. *Opt. Quantum Electron.* **2020**, *52*, 199. [[CrossRef](#)]
41. Mishra, G.P.; Kumar, D.; Chaudhary, V.S.; Kumar, S. Design and Sensitivity Improvement of Microstructured-Core Photonic Crystal Fiber Based Sensor for Methane and Hydrogen Fluoride Detection. *IEEE Sens. J.* **2022**, *22*, 1265–1272. [[CrossRef](#)]
42. Pathak, A.K.; Rahman, B.M.A.; Viphavakit, C. Nanowire Embedded Micro-Drilled Dual-Channel Approach to Develop Highly Sensitive Biosensor. *IEEE Photonics Technol. Lett.* **2022**, *34*, 707–710. [[CrossRef](#)]
43. Nwosu, F.O.; Saliu, O.D.; Oyinlola, K.A.; Ojo, E.O. Colorimetric Based Polysorbate Crosslinked Cellulose-Ag-Cu Nanohybrid Sensor for Urea Sensing Applications. *J. Polym. Environ.* **2020**, *28*, 1475–1483. [[CrossRef](#)]